Linear Persistent Angular Structure MRI and non-linear Spherical Deconvolution for Diffusion MRI

K. K. Seunarine[1], D. C. Alexander[1]

[1]Centre for Medical Image Computing, Department of Computer Science, University College London, London, United Kingdom

Introduction This abstract shows that Persistent Angular Structure (PAS) MRI [1] is a special case of Spherical Deconvolution (SD) [2]. This observation allows us to a) construct a linear implementation of PAS-MRI and b) exploit the optimal non-linear representation of PAS-MRI for SD. We show some experiments comparing linear and non-linear PAS-MRI and SD.

Methods SD reconstruction assumes that the diffusion MRI signal $A(\mathbf{q})$ is the convolution of the signal $R(\mathbf{q};\hat{\mathbf{x}})$ from a single fibre with orientation $\hat{\mathbf{x}}$ with the fibre orientation distribution (FOD) f i.e. $A(\mathbf{q}) = \int f(\hat{\mathbf{x}})R(\mathbf{q};\hat{\mathbf{x}})\mathrm{d}\hat{\mathbf{x}}$. SD attempts to recover this FOD by deconvolving the signal using a model for R. If we represent the FOD using a linear basis so that $f(\hat{\mathbf{x}}) = \sum_{k=1}^{K}\beta_k\psi_k(\hat{\mathbf{x}})$ then deconvolution is linear [2,3]. PAS-MRI calculates the persistent angular structure (PAS), which is the function $\tilde{\mathrm{p}}$ of a sphere that when embedded in 3-space has the Fourier transform that best fits the measurements $A(\mathbf{q}_1)\ldots A(\mathbf{q}_N)$. Thus $A(q) = r^2\int\tilde{\mathrm{p}}(\hat{\mathbf{x}})\cos(r\mathbf{q}\cdot\hat{\mathbf{x}})\mathrm{d}\hat{\mathbf{x}}$, where r is the radius of the sphere on which $\tilde{\mathrm{p}}$ is embedded in 3-space. This definition of $\tilde{\mathrm{p}}$ reveals that $\tilde{\mathrm{p}}$ comes from a deconvolution of the measurements using $R(\mathbf{q};\hat{\mathbf{x}}) = r^{-2}\cos(r\mathbf{q}\cdot\mathbf{x})$. The original implementation of PAS-MRI uses the maximum entropy parameterization $\tilde{p}(\hat{\mathbf{x}}) = (\lambda_0 + \sum_{j=1}^{N}\lambda_j\cos(r\mathbf{q}_j\cdot\hat{\mathbf{x}}))$. The parameters λ_j are calculated for each voxel by fitting $\tilde{p}$ to the measurements using a Levenberg-Marquardt algorithm. A non-linear implementation of SD (Maximum Entropy SD) can be obtained in a similar way [4]. The evaluation uses 12 synthetic datasets. Each dataset uses a variation of the test function $p = aG(\mathbf{x};\mathbf{D}_1,t) + (1-a)\mathbf{R}_\theta^T G(\mathbf{x};\mathbf{D}_2,t)\mathbf{R}_\theta$, where a is a mixing parameter, $G(\mathbf{x};\mathbf{D},t)$ is a zero mean Gaussian with covariance $2t\mathbf{D}$, $\mathbf{D}_1 = \mathrm{diag}(\lambda_1, \lambda_2, \lambda_2)$, $\mathbf{D}_2 = \mathrm{diag}(\lambda_2, \lambda_1, \lambda_2)$ and $\mathbf{R}_\theta$ is a rotation by θ about the z-axis. We use each combination of $\lambda_2 \in \{1,3,5\}\times 10^{-10}$ m^2/s, $a \in \{0.5,0.6\}$ and $\theta \in \{0,22.5^\circ\}$. Each dataset contains 256 sets of measurements with independent noise. The data is synthesized by sampling the Fourier transform of p at each wavenumber in a spherical acquisition scheme with 54 gradient directions and b=1154 s mm^{-2}. Noise is added to the measurements as random complex numbers with independent real and imaginary parts drawn from $N(0,\alpha^2)$, where $\alpha = F(0)/S$, F is the Fourier transform of p at each wavenumber, S is the signal to noise ratio (SNR) at b=0. We then take the modulus to get the synthetic measurement. The data generated uses S=16, which is typical of diffusion MRI data. To assess the performance of each algorithm, we compute the angle bias and direction concentration of the estimated fibre orientations for each dataset. The angle bias (α) is the angle between the mean fibre-orientation estimate from the reconstruction and the actual fibre orientation. The closer the angle bias is to zero the more accurate the estimate. The direction concentration (γ), defined in [4], is inversly related to the variance of the fibre orientation estimates. The average angle bias and average direction concentration were calculated by averaging α and γ over all 12 datasets. The linear implementations of both algorithms were optimized by varying $r \in$ [0.8,4], $bd \in$ [0.8,40] and the width of the basis functions σ so that the average angle bias was minimised. 246 basis function centres were used for both of the linear methods, as suggested in [5]. For non-linear PAS-MRI, the parameter r was set to 1.4. MESD was set so that bd = 1.

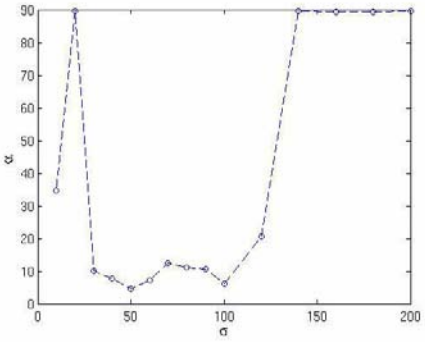

Figure 1 – Plots the average angle bias against σ for linear PAS-MRI (r=4) showing that there is a stable range of σ over which the performance varies little.

Results There is a stable range of values of σ in which the performance varies little, both in terms of angle bias and direction concentration. Figure 1 demonstrates this for linear PAS-MRI. The optimal settings for linear PAS-MRI are r=4 and σ=50. For linear SD, the optimal parameters are bd=4 and σ=40. Figure 2 shows a full set of results for both the linear and non-linear implementations. The non-linear results are for illustration only, since the non-linear methods have not been optimized.

Discussion and Conclusions The non-linear implementations of PAS-MRI and SD have a much better performance than the linear implementations in terms of the direction concentration. In terms of the angle bias, the linear methods perform better for non-orthogonally crossing fibres. However, the non-linear methods are far better at correctly estimating the number of fibre populations present in a voxel; they have fewer false positives than the linear implementations. It is worth noting that the non-linear methods still need to be optimized with regard to the parameters bd (for SD) and r (for PAS-MRI). Currently the non-linear methods are too computationally expensive, although improvements in hardware will overcome this problem.

References [1] Jansons, K. M., *et al*, Inverse Problems, 19:1031-1046, 2003. [2] Tournier, J. D., *et al*, NeuroImage, 23:1176-1185, 2004. [3] Alexander, D. C. , Annals of the New York Academy of Sciences, In Press, 2005. [4] Alexander, D. C., Proc IPMI, 2005. [5] Seunarine K. K. et al, Proc. BCISMRM, 2005.

Acknowledgements This work is funded by the EPSRC grant GR/T22858/01

$\lambda_2/10^{-12}$ (ms^{-2})	A	θ (degrees)	PAS-MRI (r=1.4)		MESD (bd=1)		Lin PAS-MRI (r=4, σ=50)		Lin SD (bd=4, σ=40)	
			Dir. Con	Angle Bias	Dir. Con	Angle Bias	Dir. Con	Angle Bias	Dir. Con	Angle Bias
100	0.5	22.5	2.5	10.4	5.5	9.2	2.9	1.3	3.2	0.9
100	0.5	0	5.6	0.2	5.9	0.2	2.4	1.8	2.9	1.0
100	0.6	22.5	3.4	9.0	5.2	12.6	2.5	2.1	2.8	0.8
100	0.6	0	5.3	0.2	5.6	0.2	2.0	2.8	2.5	1.3
300	0.5	22.5	3.7	1.9	4.0	10.0	1.6	4.6	1.9	3.4
300	0.5	0	4.3	0.4	4.7	0.4	1.7	3.7	1.9	2.8
300	0.6	22.5	3.7	3.6	3.8	13.2	1.7	1.9	1.9	1.0
300	0.6	0	4.2	0.5	4.4	0.4	1.7	2.2	1.8	1.9
500	0.5	22.5	1.8	9.8	2.0	15.1	1.3	7.7	1.4	14.6
500	0.5	0	2.1	2.2	2.3	3.1	1.4	4.5	1.5	5.6
500	0.6	22.5	1.6	12.8	1.9	15.2	0.6	14.5	1.4	6.0
500	0.6	0	2.0	2.1	2.3	2.5	1.3	7.9	1.4	5.6

Figure 2 – Results of both linear and non-linear PAS-MRI and SD. The linear implementations of these algorithms have been optimized.